Computing fast and reliable gravitational waveforms of binary neutron star merger remnants

Paul J. Easter,[1,2,*] Paul D. Lasky,[1,2,†] Andrew R. Casey,[1,2,3,‡] Luciano Rezzolla,[4] and Kentaro Takami[5]

[1]*School of Physics and Astronomy, Monash University, Victoria 3800, Australia*
[2]*OzGrav: The ARC Centre of Excellence for Gravitational Wave Discovery, Clayton Victoria 3800, Australia*
[3]*Faculty of Information Technology, Monash University, Victoria 3800, Australia*
[4]*Institut für Theoretische Physik, Max-von-Laue-Straße 1, 60438 Frankfurt, Germany*
[5]*Kobe City College of Technology, 651-2194 Kobe, Japan*

(Received 26 November 2018; published 7 August 2019)

Gravitational waves have been detected from the inspiral of a binary neutron-star, GW170817, which allowed constraints to be placed on the neutron star equation of state. The equation of state can be further constrained if gravitational waves from a postmerger remnant are detected. Postmerger waveforms are currently generated by numerical-relativity simulations, which are computationally expensive. Here we introduce a hierarchical model trained on numerical-relativity simulations, which can generate reliable postmerger spectra in a fraction of a second. Our spectra have mean fitting factors of 0.95, which compares to a fitting factor of 0.93 between different numerical-relativity codes that simulate the same physical system. This method is the first step towards generating large template banks of spectra for use in postmerger detection and parameter estimation.

DOI: 10.1103/PhysRevD.100.043005

Gravitational waves have been observed from the inspiral of binary neutron star merger GW170817 [1]. This allowed limits to be placed on the neutron star tidal deformability (see, e.g., [1–6]). However, due to a lack of detector sensitivity at high frequencies, the merger and postmerger signals were not detected [6–8]. Postmerger gravitational waves from a binary neutron star merger could be detected with a signal-to-noise ratio of 5 at a distance of ∼25–40 Mpc with Advanced LIGO at design sensitivity [9]. The physics of the postmerger remnant is of particular interest as it probes the neutron star equation of state at significantly higher temperatures than the progenitor stars.

The detection and characterization of a postmerger remnant is aided by a large bank of gravitational-wave strain waveforms. Generating such waveforms is currently computationally expensive, and there are only of order 100 in existence. In this work we make a step towards generating a large template bank of postmerger spectra by training a hierarchical model on a set of numerical-relativity spectra.

There has been significant research applied to the relationship between postmerger numerical-relativity simulations, the corresponding spectrum of the gravitational-wave strain, and the neutron star equation of state (e.g., [9–24]). There are many degrees of freedom for each simulation, which include the neutron star system parameters, equation of state, and simulation parameters (e.g., spacetime evolution formalism [25] and resolution), as well as parameters related to magnetic fields and neutrinos. We choose to use a set of numerical-relativity simulations that are homogeneous, eliminating unwanted variations between simulations with different parameters. To achieve this, we use a subset of 35 waveforms from Rezzolla and Takami [17] consisting of identical simulation parameters with variations in the neutron star mass and equation of state only. To obtain consistent spectra, we select waveforms that have a fixed time step and almost identical length.

Clark *et al.* [16] showed that dimensional reduction of postmerger waveforms is possible by performing principal component analysis after aligning the maximum of each gravitational-wave strain spectra in the frequency domain (see also [24]). We use a similar method of frequency shifting in our model. We introduce a hierarchical model that trains on existing numerical-relativity postmerger simulations and can produce new, accurate spectra in a fraction of a second. This is the first step towards making large template banks of postmerger spectra suitable for detection and parameter estimation which could complement existing unmodeled searches for postmerger remnants [6,26,27].

Simulation of the postmerger stage of binary neutron star mergers is significantly more complicated than the inspiral

*paul.easter@monash.edu
†paul.lasky@monash.edu
‡andrew.casey@monash.edu

stage due to complex physics including shock heating and nonlinear mode coupling. Additional effects, such as neutrino cooling and magnetic fields, are not expected to yield substantial modifications to the locations of the spectral peaks (see, e.g., [28–30]), while the role of viscous effects is still a matter of debate [31]. The accuracy of the resulting simulations can be limited by the trade-off between computational constraints and higher resolutions [25]. This is particularly true for the phase evolution of the postmerger simulations which do not necessarily converge [22]. However, the power-spectral content is convergent for sufficiently high resolutions (e.g., [15,22]). Our model is representative up to the validity of the numerical-relativity simulations that it is based upon. With this in mind, we wish to encourage further research into numerical-relativity simulations of postmerger remnants to increase the available number of waveforms and to enable further cross-checking between codes.

We use 35 numerical-relativity simulations of binary neutron star mergers from Rezzolla and Takami [17], to which we refer for details on the equations of state employed. Each simulation consists of nonspinning, equal-mass progenitor neutron stars, with five different equations of state across the simulations. We train our model on the amplitude of the characteristic strain spectra, $h_c(f) = |\tilde{h}(f)|\sqrt{f}$. Here, $\tilde{h}(f)$ is the Fourier transform of the plus polarization of the postmerger gravitational-wave strain, $h_+(t > 0)$. The plus and cross polarizations of the simulated gravitational-wave strain have almost identical spectral amplitude and have a phase offset of almost exactly $\pi/2$. We gain no extra information by including the cross polarization. The merger time $t = 0$ is defined as the time where $h_+^2(t) + h_\times^2(t)$ reaches the first maximum.

We use a hierarchical model to represent the amplitude spectra. Given a neutron star of mass M and radius R, we assume the compactness of a neutron star, $C \equiv M/R$, in the jth simulation has a power-law dependence with the mass M over all equations of state:

$$C_j = \alpha_j M_j^{\beta_j}. \tag{1}$$

The validity of this model will be determined by how well we can match the numerical-relativity waveforms. The hyperparameters $\{\mathbf{a}, \mathbf{b}\}$ and the quadrupolar tidal coupling constant κ_2^τ determine the values of $\{\alpha, \beta\}$ as follows:

$$\alpha_j \sim \mathcal{N}(a_0 + a_1\kappa_{2,j}^\tau, \sigma_\alpha^2), \tag{2}$$

$$\beta_j \sim \mathcal{N}(b_0 + b_1\kappa_{2,j}^\tau, \sigma_\beta^2), \tag{3}$$

where $\mathcal{N}(\mu, \sigma^2)$ is a Gaussian distribution of mean μ and variance σ^2. The quadrupolar tidal coupling constant κ_2^τ is used due to its importance in the inspiral dynamics [9,12,14,15,17,32] and its correlation with the location of the main frequency peak of the postmerger spectrum [9,11,14,15].

All spectra in the training set, which excludes the spectrum under test when leave-one-out cross-validation is performed, are used to determine the hyperparameters $\{\mathbf{a}, \mathbf{b}\}$ by a least squares fit. The amplitudes for each spectrum are frequency shifted so that the peak frequencies are aligned in a similar way to Refs. [16,24]. We then fit the aligned spectral amplitudes with a linear model

$$(h_c)_{i,j} = \mathbf{\Theta}_i \mathbf{X}_j + \text{noise}, \tag{4}$$

where the noise is modeled as intrinsic variance, s_i^2 for the ith frequency bin, $\mathbf{\Theta}_i$ is a vector of unknown coefficients, and $\mathbf{X}_j$ is a design matrix of

$$\mathbf{X}_j = [1, \hat{C}(M_j, \kappa_{2,j}^\tau), \hat{M}_j, \widehat{\kappa_{2,j}^\tau}]. \tag{5}$$

The hats indicate the whitened transformations of the neutron star parameters such that $\hat{\mathbf{x}} \sim \mathcal{N}(0,1) = (\mathbf{x} - \mu_x)/\sigma_x$, where μ_x and σ_x^2 are the mean and variance of $\mathbf{x}$, respectively. The compactness parameter can be generated from Eqs. (1)–(3) after determining the values for a_0, a_1, b_0, and b_1. Spectra can then be trivially generated given any mass, quadrupolar tidal coupling constant and frequency shift. The frequency shift can be determined from the value of the quadrupolar tidal coupling constant [14,15].

We perform leave-one-out cross-validation to test the performance of the model. We do this by excluding the spectrum under test and its associated parameters from the training set. In doing so, the spectra generated during leave-one-out cross-validation represent an extrapolation by the model and the fitting factors are therefore conservative.

We perform spectral comparisons using the following noise-weighted fitting factor, or overlap [33]:

$$FF(h_1, h_2) \equiv \frac{\langle h_1|h_2\rangle}{\sqrt{\langle h_1|h_1\rangle\langle h_2|h_2\rangle}}. \tag{6}$$

Here, the inner product is defined by

$$\langle h_1|h_2\rangle \equiv 4\int df \frac{|\tilde{h}_1(f)||\tilde{h}_2(f)|}{S_h(f)}, \tag{7}$$

where S_h is the noise power spectral density. Throughout this article we use the ZERO_DET_high_P file from [34] to determine the amplitude of S_h. The resultant fitting factor is similar to the standard fitting factor except that it operates on the Fourier amplitude only. A fitting factor of one represents a perfect match. The fitting factor represents the loss incurred to the optimal signal-to-noise ratio due to mismatch in the model spectra, where the optimal signal-to-noise ratio is given by $\rho_{\text{opt}} = \sqrt{\langle h|h\rangle}$.

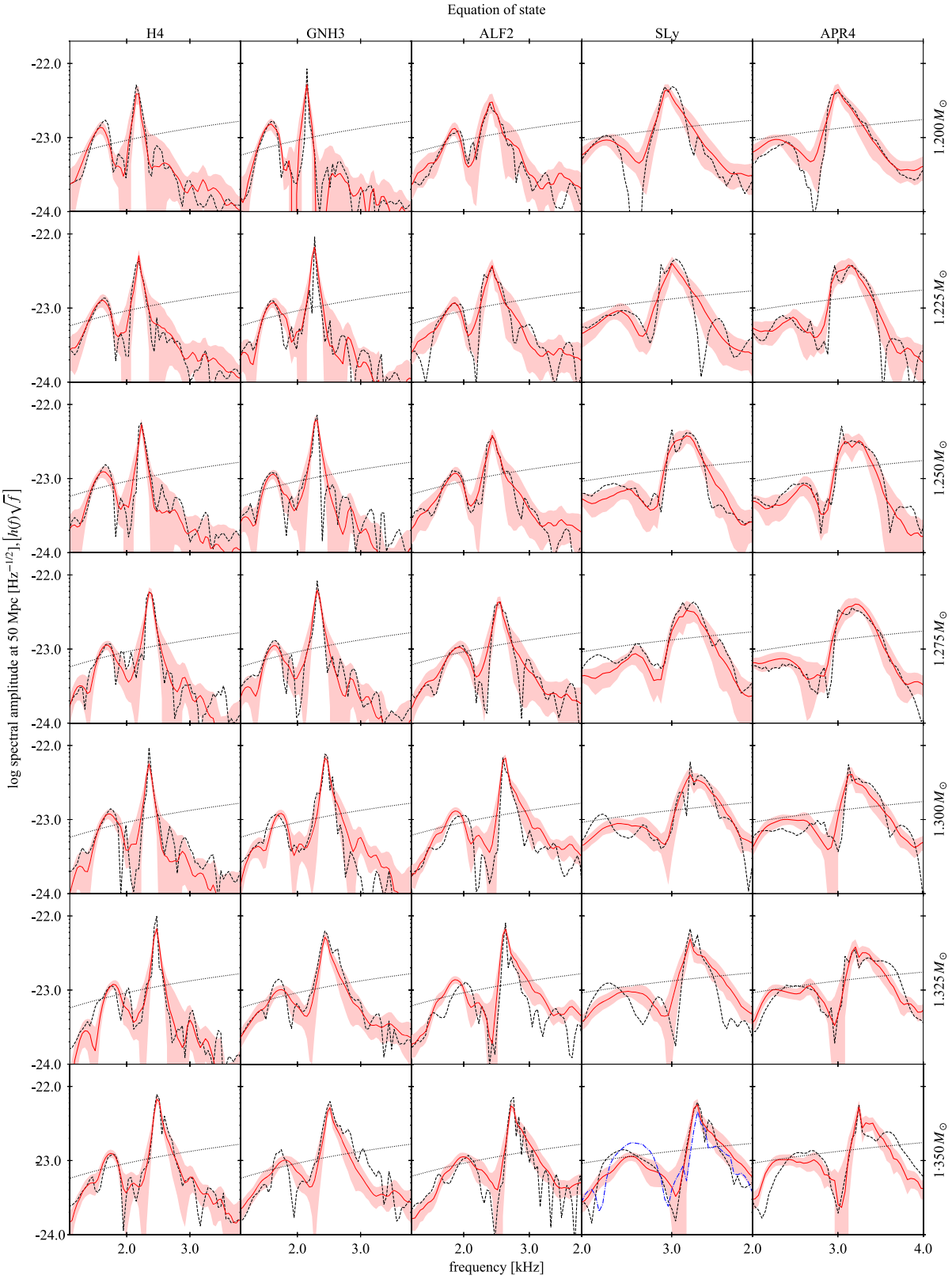

FIG. 1. Reconstructed gravitational-wave spectra generated with leave-one-out cross-validation (solid red curve) and original numerical-relativity spectra [17] (dashed black curve), scaled to a distance of 50 Mpc. Each column represents a different equation of state and each row represents a different neutron star mass, increasing towards the bottom. The one-sigma uncertainty in the spectra is shaded in light red for each prediction. The Advanced LIGO noise amplitude spectral density (dotted black curve) [34] is shown on all subplots. A numerical-relativity spectrum generated from [22] is shown (dashed dot blue curve) in the last row (equal mass 1.35 $M_\odot$) for SLy [37] (fourth column) equation of state.

While it is known that smooth relationships exist between various system properties (e.g., mass, tidal parameters, etc.) and postmerger waveform spectral features [9,11,14,15,17,35], no such relationships exist for the phase information (see also [36]). Empirically, while we find good training fits using our model on the spectral content of the waveforms (see below), we are not able to train confidently on the full time series including both phase and amplitude as the phase evolves too quickly between adjacent simulations. We discuss this in more detail below.

Following the training step, we use Eq. (4) to generate spectra. Figure 1 shows how well our generated spectra match the original numerical-relativity spectra. The original spectra are shown as dashed black curves, the cross-validation spectra are shown as red curves, and the one-sigma model uncertainty is shown in shaded light red. All spectra are scaled to a distance of 50 Mpc. The Advanced LIGO noise amplitude spectral density is shown as the dotted black curves [34]. We fit the large-scale structure of the numerical-relativity peaks well with some deviations in the small-scale structure.

Figure 2 shows a histogram of the noise-weighted fitting factor, Eq. (6), between our cross-validated model prediction and the corresponding numerical-relativity spectra for all tested waveforms. The resulting histogram has a mean of 0.95 with a standard deviation of 0.03.

To place the above results in context, we calculate the nearest neighbor fitting factor of the numerical-relativity spectra. We measure the fitting factor for the spectrum under test against all other spectra and report the largest fitting factor. We obtain nearest neighbor fitting factors for the numerical-relativity spectra of 0.93 with a standard deviation of 0.05. The fitting factors generated by our model compare favorably with this result. Additionally, our model is capable of generating spectra given the required input parameters, whereas a nearest neighbor interpolation would not be capable of this.

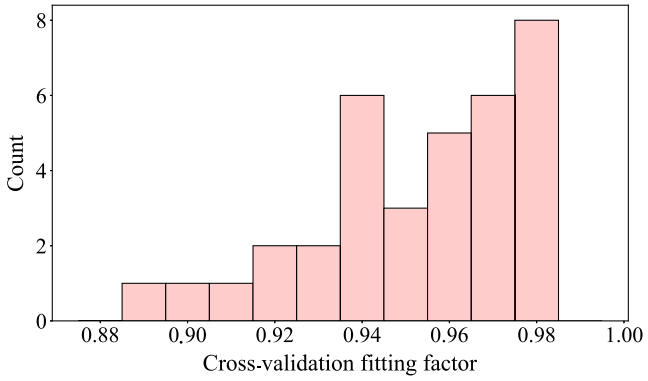

FIG. 2. Histogram of fitting factors determined by comparing numerical-relativity spectra with spectra generated by our model using leave-one-out cross-validation.

As an additional baseline value for comparison, we compare fitting factors between the numerical-relativity spectra used in this paper [17] and those produced with other codes [22]. Notwithstanding the fact that postmerger waveforms can differ with resolution even when using the same code, we assume that the waveforms have similar truncation errors and compare one set of spectra using equations of state SLy [37] for equal-mass binaries with $M = 1.35\ \mathrm{M}_{\odot}$.

The spectrum for the comparison waveform is plotted (blue dashed dot curve) in the last row and fourth column of Fig. 1, corresponding to the SLy equation of state. This spectrum can be compared to the black dashed waveform from [17] in the same panel. While amplitude offsets do not change the fitting factor, differences in the frequency and the shape of the peaks do. The fitting factor between these two waveforms is 0.93. This can be attributed to the difference in the relative shapes of the two main peaks between the simulations in [17,37].

This comparison indicates that our fitting factors are comparable to the fitting factors between different numerical-relativity codes. We note that numerical simulations are indeed accurate enough for understanding the main structures (e.g., positions of dominant peaks) and their relationship with bulk properties of the remnant. However, our method is limited by the accuracy of the numerical-relativity simulations, which are in turn limited by computational capabilities; we discuss the implications of this below.

To evaluate how the generated spectra vary, we train on all numerical-relativity spectra and generate a grid of model spectra. We generate spectra at five equally spaced mass and quadrupolar tidal coupling constant values. The mass ranges from $M = 1.25$ to $1.35\ \mathrm{M}_{\odot}$, and the quadrupolar tidal coupling constant varies from $\kappa_2^{\tau} = 50$ to 350. The generated spectra are shown in Fig. 3 as the red curves, the one-sigma model uncertainty as light red shading, and the Advanced LIGO noise curve as dotted black. Each of these spectra take a fraction of a second to evaluate. We show these spectra to indicate what we can hope to achieve by implementing these models in full parameter estimation.

In Fig. 4 we compare the fitting factor between a spectrum generated with $M = 1.3\ \mathrm{M}_{\odot}$, $\kappa_2^{\tau} = 100$ against spectra generated at other parameter values. We choose $\kappa_2^{\tau} = 100$ (for an equal-mass system this corresponds to $\Lambda = 530$) to be consistent with tidal deformability values, Λ, determined in [1–6], under the simplified assumption that $\kappa_2^{\tau} \approx \frac{3}{16}\Lambda$ (noting that the equality holds for equal-mass progenitors). The location of the reference spectrum is shown with the black cross. This provides the first indication of whether this model could recover the mass and quadrupolar tidal coupling constant when trained on sufficient numerical-relativity simulations. The peak of the contour plot around the reference waveform shows that this model is selective and may be used for parameter

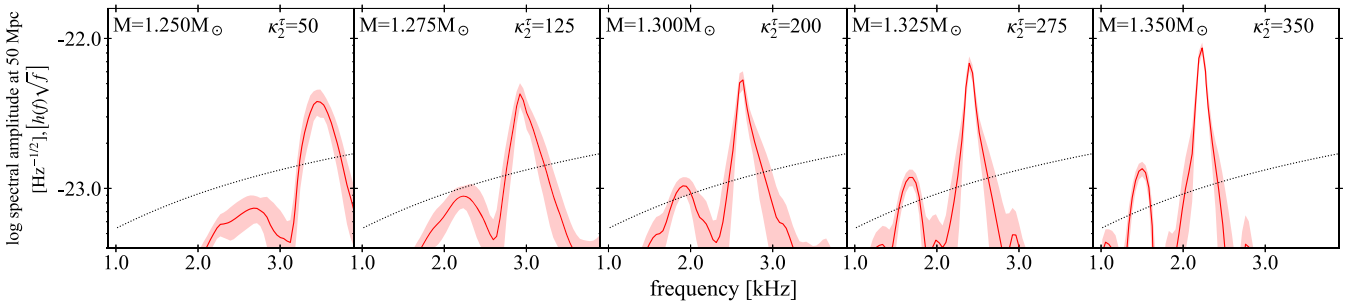

FIG. 3. Spectra generated by the model when trained on all the numerical-relativity spectra (red curve). The uncertainties in the spectra are shown in light red. The Advanced LIGO noise amplitude spectral density (dotted black line) is shown on all subplots.

estimation and/or detection in the future. However, this is a task for future work and will require full Bayesian analysis with a noise implementation.

It is possible that a phase transition may occur in the remnant during the postmerger stage due to an increase in density (e.g., [4,38]). This could be detected by comparing the inferred values of the quadrupolar tidal coupling constant from the inspiral and postmerger stages. Simulations that compare hydrodynamic models with and without quark deconfinement show that the presence of quark deconfinement causes no change in the inspiral gravitational-wave signal due to the low densities involved. This is contrasted to the postmerger stage where the densities are greater, leading to a higher proportion of deconfined quarks when modeled, which in turn leads to a change in the postmerger gravitational-wave strain [39]. Phase transitions due to quark deconfinement could be detected by training our model on simulations that disallow quark deconfinement. If a postmerger signal was detected that contained the signature of quark deconfinement, then this would result in an inconsistency between the tidal coupling constant inferred from the postmerger gravitational-wave spectra and the inspiral stage. We note that other mechanisms, either physical or arising from errors in the modeling, could also cause such frequency shifts. We leave the exploration of this as future work.

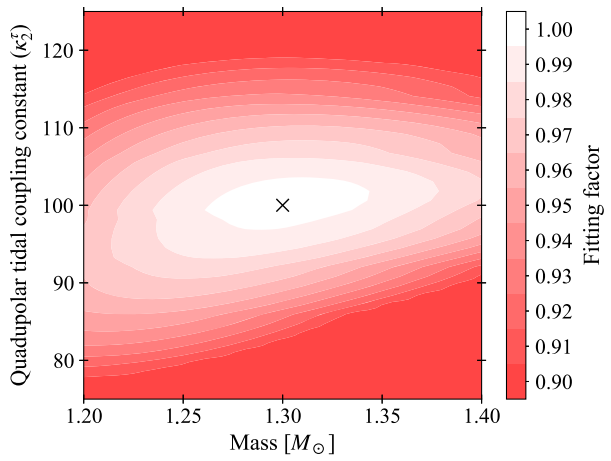

FIG. 4. Fitting factor between spectra generated using our hierarchical model with 1.30 $M_\odot$ and $\kappa_2^T = 100$ (black cross), against a grid of mass and quadrupolar tidal coupling constant values.

In this paper, we use a hierarchical model to generate binary neutron star postmerger spectra by training on spectra generated with numerical-relativity simulations. Our trained model allows us to generate spectra in $\sim 10^{-4}$ s, which significantly reduces the computational effort required to populate a template bank of spectra. We obtain noise-weighted, amplitude-only fitting factors across all tested spectra, with a mean of 0.95 and a standard deviation of 0.03. This compares favorably to a postmerger fitting factor of 0.93 between different numerical-relativity codes.

Training on the phase of the postmerger spectra will allow fitting-factor comparisons with both the amplitude and phase information, as well as the generation of time-based waveforms. In addition, it will provide insight on the number of numerical-relativity simulations required to achieve a complete and accurate database. While obtaining information on the phase evolution is in principle possible (see, e.g., [24]), this also requires a systematic investigation that goes well beyond the scope of this work. Without the phase information, a matched filter search is less sensitive, but it is still possible to design such a search using only the signal amplitudes.

Results based on our trained model suggest that the model is selective and could potentially be used in parameter estimation of detected events. If posteriors for the mass and tidal coupling constant are able to be determined, then it is a simple step to calculate the posteriors for the compactness, Eq. (1), and the radius of the neutron star. This will be confirmed in future work using a Bayesian framework. Parameter estimation of the postmerger spectra could set bounds on the postmerger quadrupolar tidal coupling constant, allowing comparison with the inspiral value. This could determine whether a phase change in the equation of state is present [38,39].

To be valuable in search and parameter-estimation studies, our model must be extended to include individual values of mass, spins, compactness and quadrupolar tidal deformabilities for each progenitor. This paper trained on

waveforms with progenitor κ_2^τ values ranging from 50 to 350 and equal-mass progenitors from 1.2 to 1.35 $M_\odot$. The merger of two progenitors with the same parameters (C, M, κ_2^τ) but different equations of state could produce different output spectra, for example if one equation of state had a lower maximum, nonrotating neutron star mass. This could be a problem for the existing model and an additional input parameter may be needed to remove the degeneracy in the output spectra. This is not necessary for the numerical-relativity simulations that are used in this paper, as there is enough variation in the three parameters to define the output spectra. The model may be also expanded to include simulations with black hole progenitors. In this case the dominant postmerger frequency, corresponding to black hole ringdown, would likely be too high for detection with Advanced LIGO. These changes can be introduced given enough numerical-relativity simulations to cover the required ranges of parameter values. The placement of numerical-relativity simulations to enable this is a subject of future work. Our method may eventually provide an additional tool to aid in the detection of short-term postmerger neutron star remnants, supplementing the existing tools [26,27].

ACKNOWLEDGMENTS

P. D. L. is supported through Australian Research Council (ARC) Future Fellowship No. FT160100112 and ARC Discovery Project No. DP180103155, and A. R. C. is supported in part by the Australian Research Council through Discovery Grant No. DP160100637. We thank James Clark and Eric Thrane for their feedback.

[1] B. P. Abbott, R. Abbott, T. D. Abbott, F. Acernese, K. Ackley, C. Adams, T. Adams, P. Addesso, R. X. Adhikari, V. B. Adya *et al.*, Phys. Rev. Lett. **119**, 161101 (2017).
[2] E. Annala, T. Gorda, A. Kurkela, and A. Vuorinen, Phys. Rev. Lett. **120**, 172703 (2018).
[3] D. Radice, A. Perego, F. Zappa, and S. Bernuzzi, Astrophys. J. Lett. **852**, L29 (2018).
[4] E. R. Most, L. R. Weih, L. Rezzolla, and J. Schaffner-Bielich, Phys. Rev. Lett. **120**, 261103 (2018).
[5] S. De, D. Finstad, J. M. Lattimer, D. A. Brown, E. Berger, and C. M. Biwer, Phys. Rev. Lett. **121**, 091102 (2018).
[6] B. P. Abbott, R. Abbott, T. D. Abbott, F. Acernese, K. Ackley, C. Adams, T. Adams, P. Addesso, R. X. Adhikari, and V. B. Adya, Phys. Rev. X **9**, 011001 (2019).
[7] B. P. Abbott, R. Abbott, T. D. Abbott, F. Acernese, K. Ackley, C. Adams, T. Adams, P. Addesso, R. X. Adhikari, V. B. Adya *et al.*, Astrophys. J. Lett. **851**, L16 (2017).
[8] B. P. Abbott, R. Abbott, T. D. Abbott, F. Acernese, K. Ackley, C. Adams, T. Adams, P. Addesso, R. X. Adhikari, and V. B. Adya, Astrophys. J. **875**, 160 (2019).
[9] K. Takami, L. Rezzolla, and L. Baiotti, Phys. Rev. Lett. **113**, 091104 (2014).
[10] N. Stergioulas, A. Bauswein, K. Zagkouris, and H.-T. Janka, Mon. Not. R. Astron. Soc. **418**, 427 (2011).
[11] A. Bauswein and H.-T. Janka, Phys. Rev. Lett. **108**, 011101 (2012).
[12] J. S. Read, L. Baiotti, J. D. E. Creighton, J. L. Friedman, B. Giacomazzo, K. Kyutoku, C. Markakis, L. Rezzolla, M. Shibata, and K. Taniguchi, Phys. Rev. D **88**, 044042 (2013).
[13] K. Hotokezaka, K. Kiuchi, K. Kyutoku, T. Muranushi, Y.-i. Sekiguchi, M. Shibata, and K. Taniguchi, Phys. Rev. D **88**, 044026 (2013).
[14] S. Bernuzzi, T. Dietrich, and A. Nagar, Phys. Rev. Lett. **115**, 091101 (2015).
[15] K. Takami, L. Rezzolla, and L. Baiotti, Phys. Rev. D **91**, 064001 (2015).
[16] J. A. Clark, A. Bauswein, N. Stergioulas, and D. Shoemaker, Classical Quantum Gravity **33**, 085003 (2016).
[17] L. Rezzolla and K. Takami, Phys. Rev. D **93**, 124051 (2016).
[18] D. Radice, Astrophys. J. Lett. **838**, L2 (2017).
[19] T. Dietrich and T. Hinderer, Phys. Rev. D **95**, 124006 (2017).
[20] D. Radice, S. Bernuzzi, W. Del Pozzo, L. F. Roberts, and C. D. Ott, Astrophys. J. Lett. **842**, L10 (2017).
[21] R. De Pietri, A. Feo, J. A. Font, F. Löffler, F. Maione, M. Pasquali, and N. Stergioulas, Phys. Rev. Lett. **120**, 221101 (2018).
[22] T. Dietrich, D. Radice, S. Bernuzzi, F. Zappa, A. Perego, B. Brueugmann, S. V. Chaurasia, R. Dudi, W. Tichy, and M. Ujevic, Classical Quantum Gravity **35**, 24LT01 (2018).
[23] T. Dietrich, S. Bernuzzi, B. Brügmann, M. Ujevic, and W. Tichy, Phys. Rev. D **97**, 064002 (2018).
[24] S. Bose, K. Chakravarti, L. Rezzolla, B. S. Sathyaprakash, and K. Takami, Phys. Rev. Lett. **120**, 031102 (2018).
[25] L. Baiotti and L. Rezzolla, Rep. Prog. Phys. **80**, 096901 (2017).
[26] S. Klimenko, G. Vedovato, M. Drago, F. Salemi, V. Tiwari, G. A. Prodi, C. Lazzaro, K. Ackley, S. Tiwari, C. F. Da Silva, and G. Mitselmakher, Phys. Rev. D **93**, 042004 (2016).
[27] K. Chatziioannou, J. A. Clark, A. Bauswein, M. Millhouse, T. B. Littenberg, and N. Cornish, Phys. Rev. D **96**, 124035 (2017).
[28] B. Giacomazzo, L. Rezzolla, and L. Baiotti, Phys. Rev. D **83**, 044014 (2011).
[29] Y. Sekiguchi, K. Kiuchi, K. Kyutoku, M. Shibata, and K. Taniguchi, Phys. Rev. D **93**, 124046 (2016).
[30] T. Kawamura, B. Giacomazzo, W. Kastaun, R. Ciolfi, A. Endrizzi, L. Baiotti, and R. Perna, Phys. Rev. D **94**, 064012 (2016).

[31] M. G. Alford, L. Bovard, M. Hanauske, L. Rezzolla, and K. Schwenzer, Phys. Rev. Lett. **120**, 041101 (2018).
[32] T. Damour and A. Nagar, Phys. Rev. D **81**, 084016 (2010).
[33] T. A. Apostolatos, Phys. Rev. D **52**, 605 (1995).
[34] LIGO Scientific Collaboration, Advanced LIGO anticipated sensitivity curves, 2010, https://dcc.ligo.org/LIGO-T0900288/public, ZERO_DET_high_P.txt.
[35] A. Bauswein and N. Stergioulas, Phys. Rev. D **91**, 124056 (2015).
[36] C. Messenger, K. Takami, S. Gossan, L. Rezzolla, and B. S. Sathyaprakash, Phys. Rev. X **4**, 041004 (2014).
[37] D. Radice, S. Bernuzzi, and C. D. Ott, Phys. Rev. D **94**, 064011 (2016).
[38] A. Bauswein, N.-U. F. Bastian, D. B. Blaschke, K. Chatziioannou, J. A. Clark, T. Fischer, and M. Oertel, Phys. Rev. Lett. **122**, 061102 (2019).
[39] E. R. Most, L. J. Papenfort, V. Dexheimer, M. Hanauske, S. Schramm, H. Stöcker, and L. Rezzolla, Phys. Rev. Lett. **122**, 061101 (2019).